Horizon 2020
European Union funding
for Research & Innovation

E-Infrastructures

H2020-EINFRA-2015-1

EINFRA-5-2015: Centres of Excellence for computing applications

EoCoE

Energy oriented Center of Excellence for computing applications

Grant Agreement Number: EINFRA-676629

D2.6 - M24

Formulation for optimization under uncertainty

Project and Deliverable Information Sheet

EoCoE	Project Ref:	EINFRA-676629
	Project Title:	Energy oriented Centre of Excellence
	Project Web Site:	http://www.eocoe.eu
	Deliverable ID:	D2.6
	Lead Beneficiary:	RWTH
	Contact:	Jeffrey Cumpston
	Contact's e-mail:	jeff.cumpston@avt.rwth-aachen.de
	Deliverable Nature:	Report
	Dissemination Level:	PU*
	Contractual Date of Delivery:	M24 30/09/2017
	Actual Date of Delivery:	M31 24/04/2018
	EC Project Officer:	Carlos Morais-Pires

* - The dissemination level are indicated as follows: PU – Public, CO – Confidential, only for members of the consortium (including the Commission Services) CL – Classified, as referred to in Commission Decision 2991/844/EC.

Document Control Sheet

Document	Title :	Formulation for optimization under uncertainty
	ID :	D2.6
	Available at:	http://www.eocoe.eu
	Software tool:	LaTeX
Authorship	Written by:	J. Cumpston, S. Metzger, A. Mitsos
	Contributors:	Danimir Doncevic, Linda Brodnicke, Benedikt Bier, Pai Liu
	Reviewed by:	PEC members

Contents

List of Figures

List of Tables

1. Introduction to Task

The purpose of Work Package 2 is to address and overcome central algorithmic core problems in the realm of energy meteorology, with Task 3 envisaged to transform the solar energy prediction to a prediction of optimal power generation of concentrated solar power. The title of Task 2.3 is "Optimal operation of Concentrated Solar Power (CSP) under Weather Uncertainty."

The goals of the task are to:

1. Further develop methodologies for optimal operation under uncertainty and for the first time apply these to renewable energy [RWTH]
2. Demonstrate the effect of uncertainty on optimal operation, thus setting the goals for accurately characterizing the uncertainty [RWTH]
3. Compare state-of-the-art weather prediction at the local scale with the ones developed, demonstrating the additional value. [CyI]

The research direction in this task has been lead by RWTH, with contributions from the Cyprus Institute and from Forschungszentrum Jülich.

1.1 Activity Summary

The following list contains aspects of the work performed under the EoCoE project as part of WP 2.3

1. Creation of one DNI forecast time series per hour for 48 hours, each with a time horizon of 48 hours, for use in dispatch optimisation.
2. Creation of a numerical model for optimisation of thermal energy storage scheduling in a CSP plant.
3. Creation of decision-making model for implementing optimal storage schedule subject to deviations in expected solar DNI.
4. Generation of optimised dispatch schedules subject to artificially erroneous day-ahead commitment time series that was created with systematically imposed errors in the DNI and spot price time series.
5. Simulation of power plant operation using the best-guess spot price and DNI forecasts that are inherently erroneous, with plant operation decisions made by decision-making controller to cope with deviations between forecasts DNI and real DNI.

2. Power plant model and simulation boundary conditions

The purpose of this project was to optimise the dispatch of a CSP power plant under uncertainties associated with forecasts of electricity market spot price and direct normal irradiance (DNI). The plant location is on the island of Cyprus, where aerosols can have a notable effect on the variation of DNI in clear-sky conditions.

A basic power plant model is used that is apt for optimisation using a MILP solver. We base our model on that from Dominguez et al. [2012], with the addition of a generation commitment penalty. The model code is included in Section A, and is written in the format

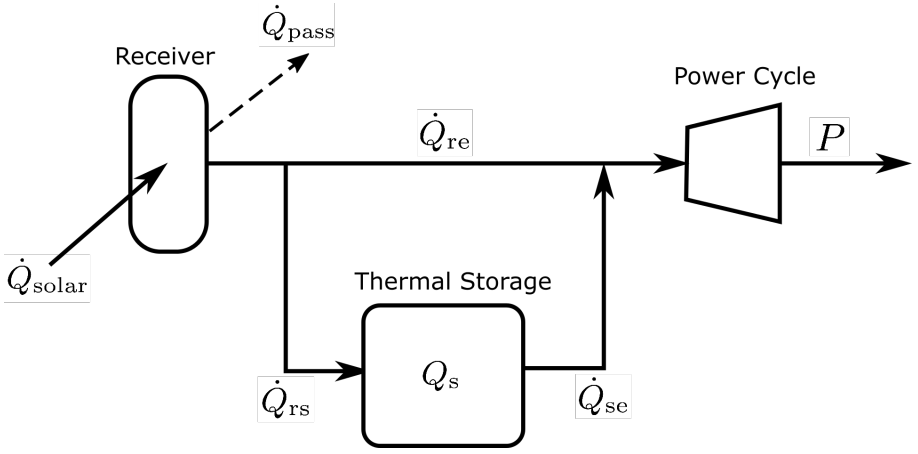

Figure 1: A basic schematic that represents the energy flows defined by the optimisation model. Energy may flow from the receiver to either the power block or to the thermal energy storage. Energy may also flow from the thermal energy storage to the power block, having been stored for a time at which dispatch conditions are more favourable.

accepted by Minizinc[1]. This plant model is solved using the g12 suite of optimisation tools. For each of the scalar and array parameters, there is an associated file that provides the necessary boundary conditions for the model. This file is in plain text, and its creation has been automated using a Python wrapper in order to run the suite of simulations necessary for this study.

A schematic of the plant appears in Figure 1. The reader should take care to note that the elements that appear in the diagram are not a complete representation of a CSP power plant, but rather a representation of the elements from which the optimisation is comprised. The thermal energy storage, for example, would typically comprise a two-tank system in which hot and cold molten salt is stored. The thermal energy storage element is represented in the model, however, by a single variable Q_{s} that represents the available stored energy. Likewise with the power cycle, represented here as a single turbine elements, and implemented in the model by an overall thermal-to-electric efficiency, η_{cycle}.

The DNI forecast time series provided by the Cyprus Institute is multiplied by a solar field optical efficiency derived from a solar field model that simulates shading, blocking, reflectivity, atmospheric attenuation, and receiver intercept. The solar field that was simulated follows the sunflower pattern first presented by Noone et al. [2012]. The field is the result of an optimisation that was performed for a plant comprised of 5000 heliostats, each with an area of 120m^2 optimised for a latitude of -33.38°, which has been inverted for operation in the northern hemisphere, given that the latitude is within 2 degrees of the latitude of Cyprus. The solar multiple of the plant is 1.5 and the chosen number of storage hours was 4.

2.1 Objective Function

Here the objective function of the power plant model is given, as it provides a useful basis for understanding how the model works, and the different influences that are investigated in subsequent sections,

[1] www.minizinc.org

$$\text{Revenue} = \Delta T \sum_{t=1}^{N_\text{T}} (P_t \text{SP}_t - C_{\Delta\text{P}} |P_t - P_{t-1}|) - \Delta T \sum_{t=1}^{N_\text{commit}} C_\text{commit} |P_{\text{commit},t} - P_t| \quad (1)$$

where Δt is the time interval for the model and is one hour in this case, N_T is the number of time steps, P_t is the power output from the turbine at time t, SP_t is the spot price at time t, $C_{\Delta\text{P}}$ is a monetary penalty for changing the output of the turbine, in this case 1 Euro/MWh, N_commit is the number of time steps remaining the period for which a generation commitment has been made, C_commit is the cost of deviation from the generation commitment, in this case 10 Euros/MWh, and P_commit is the committed power generation at time t.

The constraints on the model include maximum and minimum turbine operation, a minimum respective up and down time for the operation of the power block, and maximum and minimum tank energy storage.

2.2 Day-ahead power commitment

In the European spot price market, a day-ahead power generation commitment must be made at noon on the previous day. This power commitment estimates the generation for the 24 hours of the following day, and is based on expected generation. In the case of variable renewable energies, it represents a best estimation of generation and is usually subject to uncertainties. Subsequent generation should follow this commitment, or may be subject to a penalty that is proportional to the difference in the actual amount of generated power and the committed power. As a commitment penalty factor is included in the optimisation objective function, the optimiser is able to make a decision on whether generation is favourable at a particular time, while taking into account potential losses due this penalty. In reality, the commitment penalty is influenced by market conditions at the time-point of generation, where Figure 2 shows an example of a year of generation pentalties [Kraas et al., 2013], for which we have no model. We therefore assume a representative penalty value of 10 Euros/MWh of difference between commitment and generation.

2.3 Simulation time window

The simulations are conducted to simulate plant operation from 12:00 10/08/2016 until 12:00 12/08/2016. We begin the simulations at 12 noon in order to make a generation commitment at the first time step based upon an optimisation using the current spot price and DNI forecasts. This initial optimisation necessarily involves generation over the remaining 12 hours of the first day, over which an existing generation schedule will have already been committed. We first run the model assuming perfect forecast information to create an existing commitment P_commit for the first 12 hours of the simulation, a commitment that in reality would have been made on the previous day.

3. NWP model for DNI forecasting

This section details the contribution of the Cyprus Institute to the project in creating and providing DNI forecast time series.

Within the European Commission HORIZON 2020 project, www.EoCoE.eu, task WP2.3, Optimal Operation of Concentrated Solar Power (CSP) under Weather Uncertainty, The Cyprus Institute, has generated day-ahead forecasts of the direct normal irradiance (DNI) for the Pentakomo CSP field facility that are based on a sophisticated

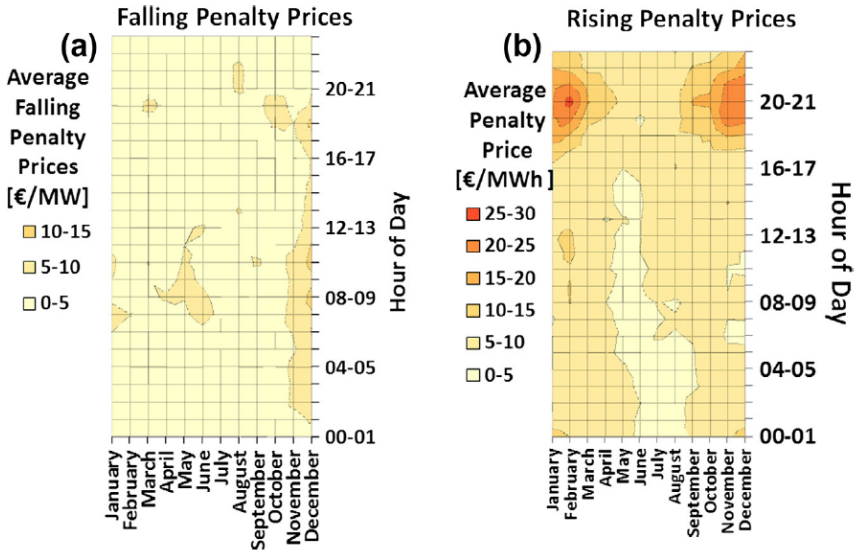

Figure 2: A contour plot representing the variation in commitment penalty prices over the course of a year for the Spanish electricity market.

coupling of WRF-solar with a "solar" version of EMAC. The augmented EMAC model results — a high resolution Earth System Model with fully coupled aerosol-chemistry-cloud-radiation feedbacks [Adbelkader et al., 2015, Abdelkader et al., 2017], which has been developed by S. Metzger, and colleagues at CyI and MPIC — show improved model results of the Aerosol Optical depth (AOD) and the Global Horizontal Irradiation (GHI), as shown in Figures 3, 4, and 5. These improvements further help to improve the DNI forecasting, since the GHI and the DNI are strongly related. Both radiative properties are largely influenced by the aerosol hygroscopic growth and the associated aerosol water (AW) mass, which often controls the atmospheric visibility, haze and the formation of clouds, especially of optically thin clouds. To allow an efficient application of a research model, we have reduced the complexity of the required aerosol chemistry and AW thermodynamics of our EMAC version to a minimum [Metzger et al., 2012, 2016a,b], so that numerical forecasts can be obtained. Subsequently, we have coupled the AOD values of EMAC, which are calculated using sophisticated aerosol-chemistry, with the cloud and radiation of WRF-solar (Figure 4) to improve DNI forecasting with WRF-solar. Our coupled EMAC-WRF-solar results have been compared with observations at Pentakomo, and against reference simulations of WRF-met, as used by the Cyprus met-office, shown in Figure 4. Additionally, we have generated 48 day-ahead forecasts (each a 48 hours prediction with a one-hour moving initialization), which are shown in Figure 5. These coupled WRF-solar results show a considerable sensitivity to the AOD values provided by EMAC, and can help to improve the DNI forecasting for certain conditions, i.e., when aerosol loadings become dominant. Further improvements of the EMAC-WRF-solar coupling might be required for DNI forecasting, which are, however, beyond the scope of this WP2.3 contribution [2].

[2]The forecasts, reference simulations and observations have been delivered to RWTH Aachen. The sub-task of CyI for WP2.3 is herewith completed. The PROTEAS facility in Cyprus has been utilized to optimize predictions for local atmospheric conditions (turbidity / visibility, humidity), as these affect the (nontrivial) irradiation attenuation relevant to GHI/DNI forecasting. The aerosol and 4-dimensional radiative model output can be further used to enhance predic-tions of the optimal energy storage schedules, subject also to market spot prices (by J. Cumptson, A. Mitsos, www.AVT.RWTH-Aachen.de) in order to

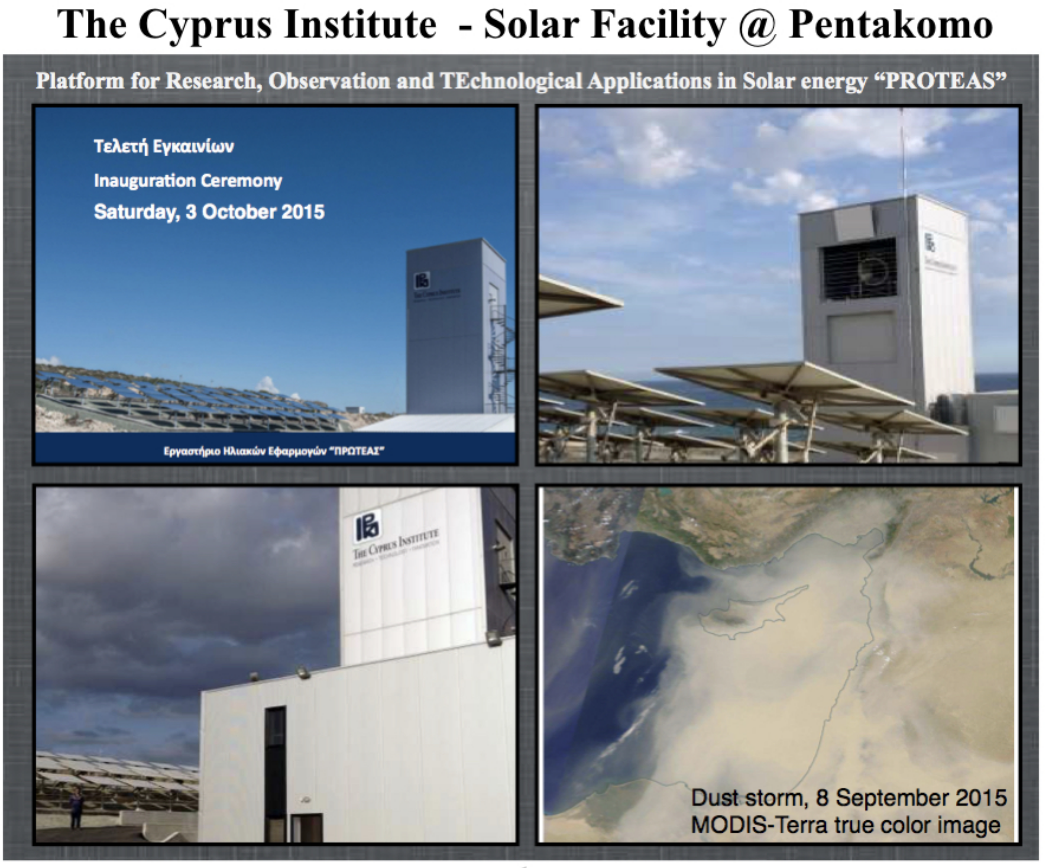

Figure 3: Map of Cyprus and model forecasts. Daily means of long-term observations (black) of the global horizontal irradiance (GHI) obtained at The Cyprus Institute's Solar Research Facility "PROTEAS", Pentakomo, and model calculations with the EMAC atmospheric chemistry-climate model (red). Overlaid (green) are the EMAC results for the Aerosol Optical Depth (AOD) - the AOD peaks nicely coincides with the GHI/DNI troughs. The high AOD peaks in spring 2015 are caused by strong outflow events of mineral dust, which is captured rather well by this high-resolution version of EMAC, which has been nudged to www.ECWMF.int ERA-Interim reanalysis data. Our EMAC aerosol version is developed and maintained at the Cyprus Institute, www.CyI.ac.cy, in close collaboration with the Max Planck Institute for Chemistry (www.MPIC.de).

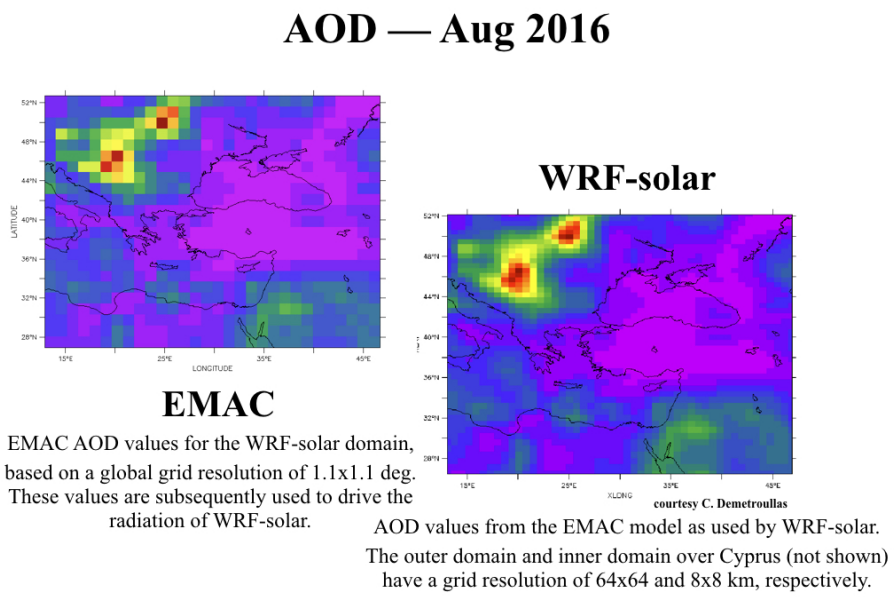

Figure 4: Coupling of EMAC and WRF-solar through AOD.

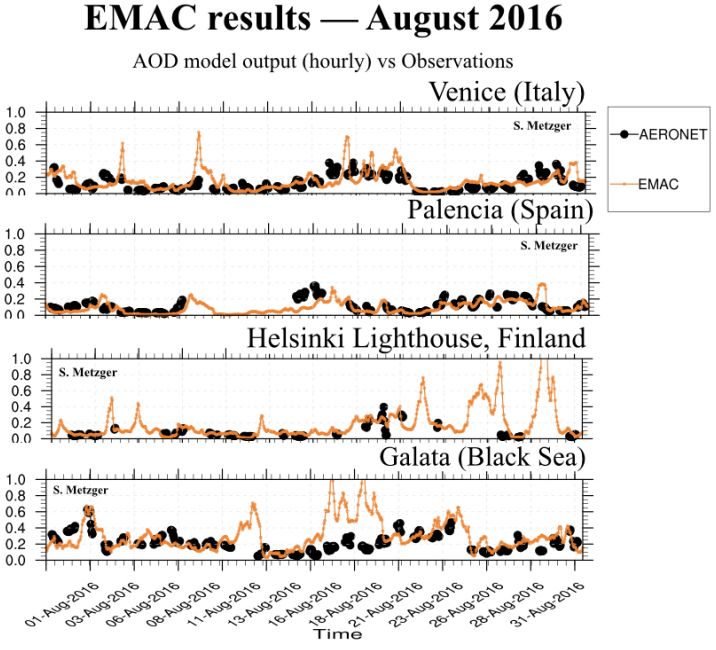

Figure 5: EMAC simulation versus AOD ground station observations.

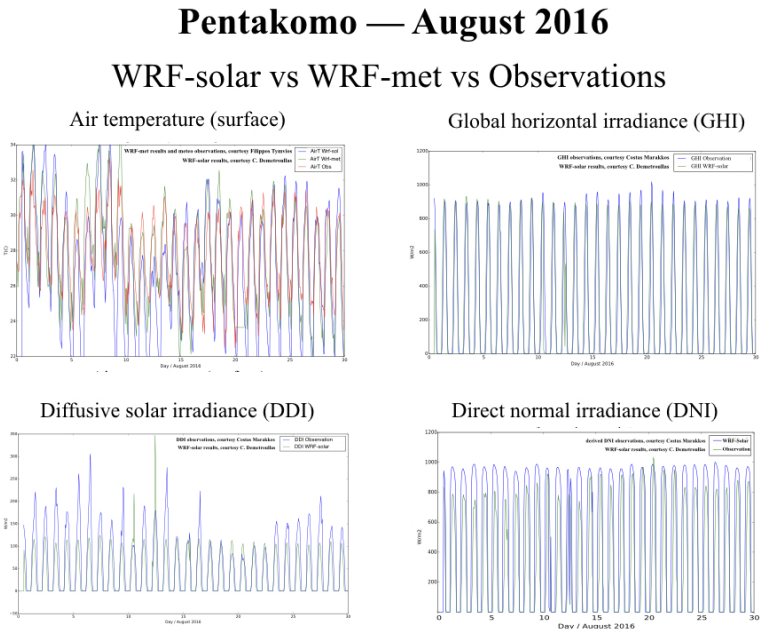

Figure 6: WRF-solar reference simulations versus WRF-met and observations.

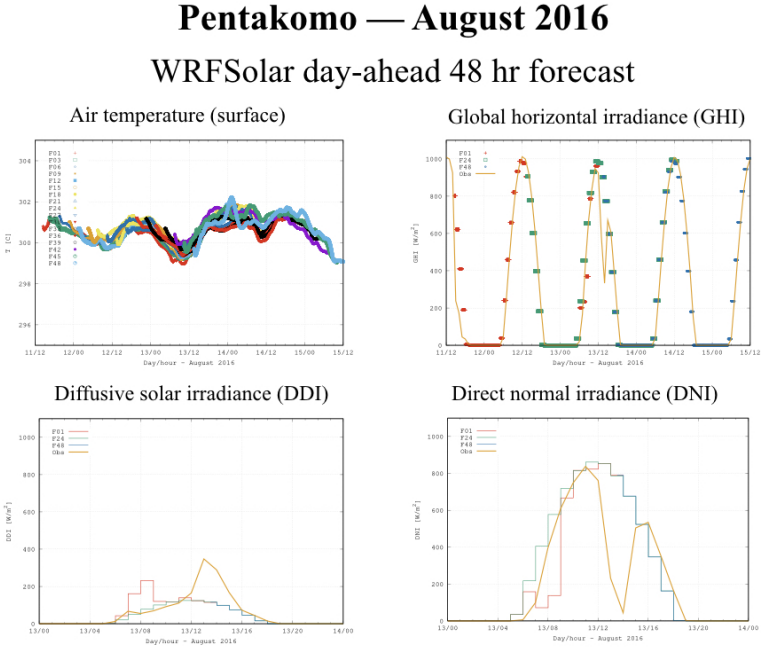

Figure 7: WRF-solar day-ahead forecasts driven by EMAC AOD.

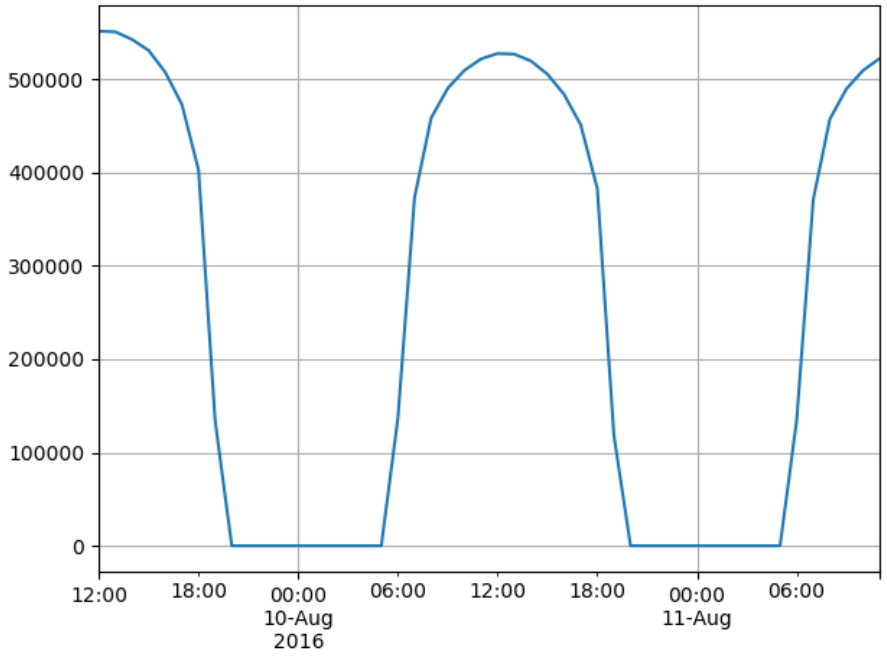

Figure 8: The time series of measured DNI values. Each time point in this this time series is built from the first time step taken from the respective rolling forecast time series.

4. Forecasting techniques and resultant time series

The purpose of the current investigation is to determine the effect that an inaccurate DNI forecast and spot price forecast has on the subsequent generation schedule and revenue of the power plant. In this section we present the techniques used to forecast a suite of time series that are used to simulate real-time operation of CSP power plants in Section 6. First, we present the results of the WRF-Solar model in generating the DNI time series, and second, the results from an ARIMA model that was trained using historical electricity market spot price data is presented.

4.1 DNI Forecast Time Series

In order to conduct this study, 48 separate time series of hourly DNI forecasts were provided. Each of the time series is separated by an hour, and therefore represents forecasts being made at hourly intervals over the period of two days. The time horizon of these forecasts is 48 hours, which allows the simulation of real-time optimisation of CSP power plant dispatch two days in advance being performed every hour over two days of operation. The subsequent "observed" DNI time series was taken from the first time step of each of the forecast time series, and is shown in Figure 8).

The DNI forecasts are overlaid upon one another in Figure 9. A close-up of the forecasts for one of the days with clear-sky conditions is shown in Figure 10. In this figure, it is evident that there is a distribution of the forecast values for a given time step. In the time series of measured values of Figure 8, only clear-sky days occur, despite some of the forecast values exhibiting drops in DNI that indicate the presence of clouds. These time

minimize costs for grid and utility operators, as well as for the general public. This collaborative work also forms the first attribution of uncertainty in plant operation to a physical cause, in this case to minimize the mirror surface error.

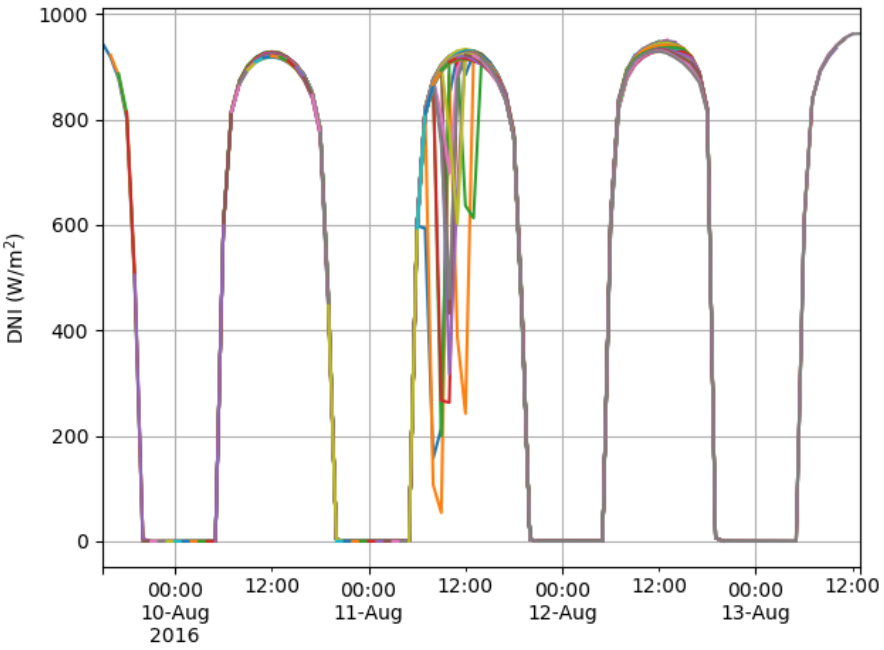

Figure 9: Forecasts of DNI data made using the WRF Solar model, with advanced aerosol modelling from the Cyprus Institute

periods of cloud cover therefore never eventuated. This is important in the investigation of Section 5.1, where a multiplier is applied to the DNI time series that is consistent with variations in DNI during clear sky conditions.

In order to investigate the effect of the forecast time horizon on the accuracy of the forecast, the standard deviation of the DNI forecasts as a function of the time interval between the current time and the predicted value is given in Figure 11, against a baseline of the measured DNI time series. Care should be taken in interpreting these plots, as they do not represent a true ensemble forecast, but rather the values from different forecast time series generated at different times. Furthermore, the use of this technique means that the number of available data points for each time-step-in-advance declines by 1 with each time step, as the later forecast time series have predictions that are outside the time-range of the measured data, such that there is no basis for comparison from which a deviation can be posited.

Referring to Figure 11, the large standard deviations observed for time horizons greater than 34 hours in advance are due to predicted cloud cover that never eventuated. Because the standard deviation of the forecasts under clear-sky conditions are far smaller, a close-up of these values is given in Figure 12.

It is expected that the further in advance a forecast is, the more the forecasts deviate from the subsequently measured value. The standard deviation does increase up to three hours ahead, and then exhibits variable behaviour thereafter. This is an artefact of the prediction technique, and it may be that the magnitude of the forecast and subsequent measured DNI in Cyprus, using the model from the Cyprus Institute described in Section 3, are accurate to a standard deviation of approximately 4 W/m^2, as observed. Under clear-sky conditions, this represents the ability to determine power plant energy availability to

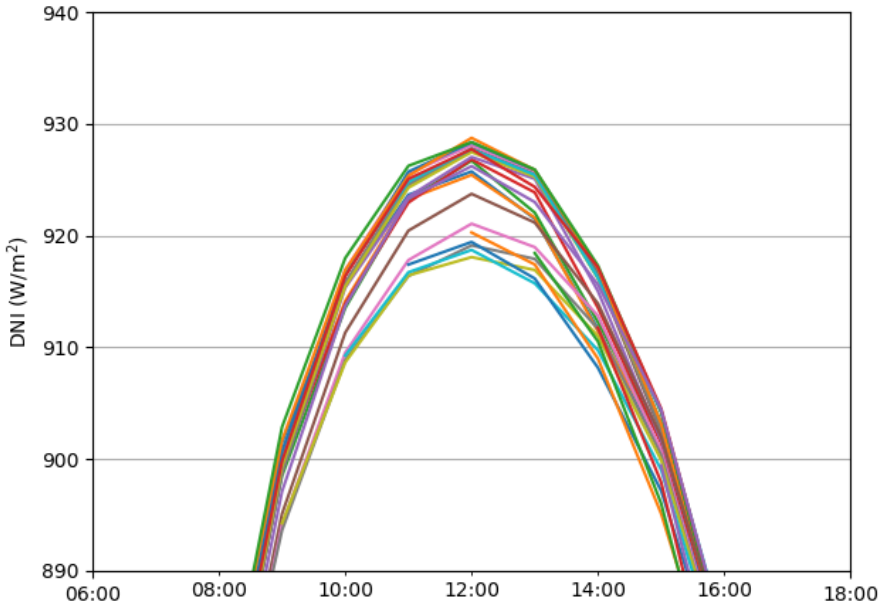

Figure 10: Close-up of forecasts shown in Fig. 9 for a time-period over which the solar DNI is peaking around midday.

an accuracy of better than 0.5%. As we are working with a limited dataset, the validity of this high forecast accuracy is a topic for further work.

4.2 Spot Price Forecasts

We use publicly available historical electricity spot price data for the Spanish market in order to inform an ARIMA model for predicting spot price data. This is displayed in Figure 13, where an example training interval and an example of a subsequent two-day price prediction is shown. Spanish market data is used for this study of the CSP in Cypriot weather conditions as while there are currently plans to open the Cypriot electricity market to spot price trading, there is currently no such market.

The suite of predicted prices used for this study are shown in Figure 14 and are overlaid on top of one another in the same way as in Figure 9. From this figure, it appears that the ARIMA model predicts the time of the price peaks to within an hour and correctly predicts maxima and minima, while the magnitude of the predicted peaks are variable.

This variation is highlighted in Figure 15, where the residual values of the spot price forecasts are plotted against a baseline of the subsequent real time series. This is important in the investigation of Section 5.1, where a multiplier is applied to the residual of the spot price time series over a baseline of the average spot price in order to simulate errors in the price peaks.

As with the DNI forecasts, the standard deviation of the forecast spot price time series is shown as a function of forecast lead time over the two days of actual operation for which rolling forecasts are available in Figure 16. We also remind the reader that less data points are available for forecasts with a greater lead time. This figure shows that the further in advance the lead time of the forecast data point is, the higher the uncertainty, up

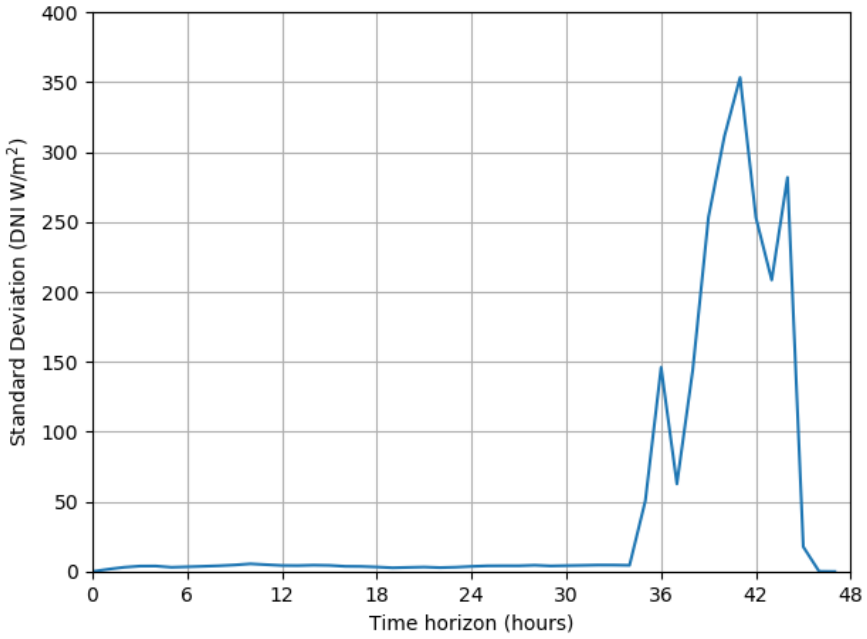

Figure 11: Standard deviation of the DNI forecasts as a function prediction time interval. The number of data points used to calculated each standard deviation varies, with less data points available for longer lead times.

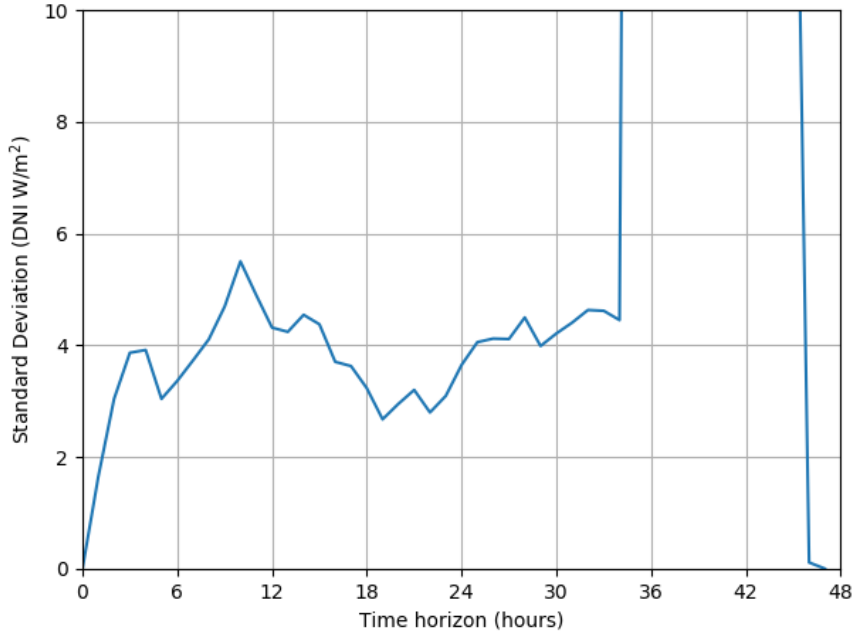

Figure 12: Closeup of the standard deviation shown in Figure 11 to emphasise the standard deviation of the data for clear sky predictions and for which a greater number of data points were available.

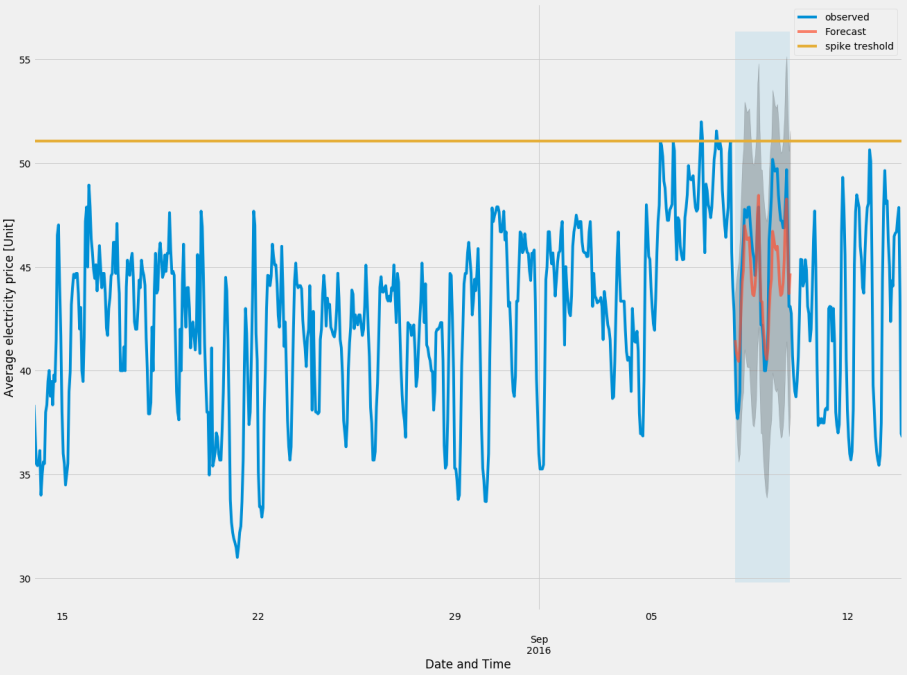

Figure 13: Forecast of the spot price made using an ARIMA model(red), overlaid on the actual spot price (blue). Uncertainties from the ARIMA model are shown in grey. An attempt at defining a spike threshold is evident (yellow) and is the topic of ongoing work.

to about 30 hours in advance, beyond which the uncertainty declines. As it is unlikely that larger lead times in the forecast values should have lower error distributions, this decline may result from the declining number of data points available for these large advances in forecast, introducing inaccuracy into the statistics. The average of the measured spot price over the two time intervals was 40.2 Euros/MWh. We therefore claim an accuracy over the two days of operation of better than 10%, subject to the aforementioned caveat for long forecast time horizons.

5. Generation schedule with incorrect commitment

In this section, we present results from the optimisation of the generation schedule when the generation commitment is incorrectly estimated.

5.1 Artificial Errors

In order to investigate the effect of uncertainty on the forecast DNI and spot prices in making generation commitments, the time series were systematically altered in a way that is consistent with the errors in forecasts that one might expect under clear sky conditions using an ARIMA model for spot price predictions.

The DNI time series was multiplied by constant factor. Normally, the shape of the DNI time series is preserved under these conditions, with the magnitude of the DNI being affected by local atmospheric conditions. The DNI multipliers used range from 0.1 to 1.2 in increments of 0.1, and Figure 17 shows the resulting time series of thermal energy incident on the receiver once the measured time series has been multiplied by these factors. For the sake of inquiry, the range of DNI multipliers that were used to generated these time series are much wider than the affects of atmospheric aerosol scattering under clear sky

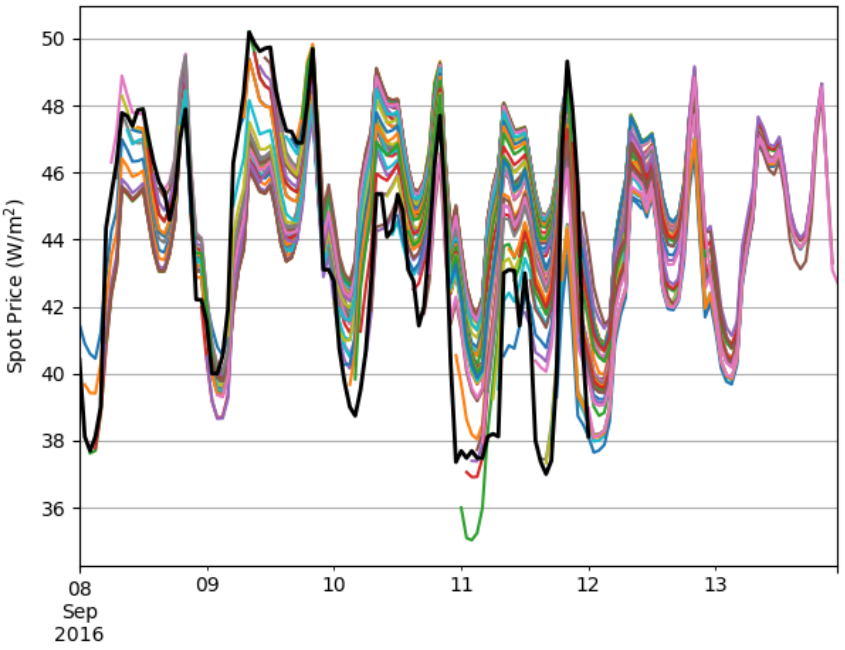

Figure 14: Forecasts of spot price from ARIMA model overlaid on one another. The peaks predicted by the model are consistent and accurate, while the magnitude of the peaks is variable.

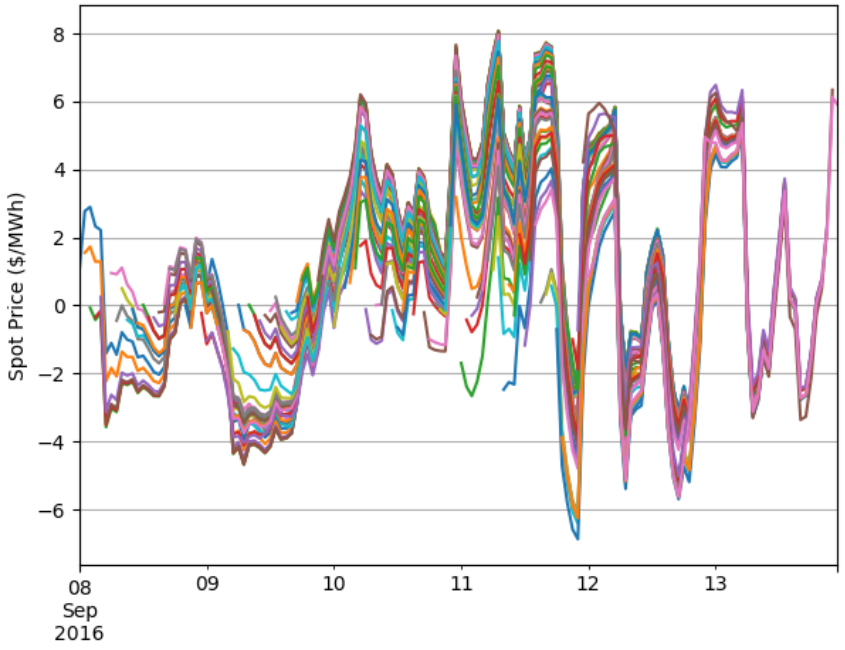

Figure 15: Residuals of spot-price forecasts when the actual spot price is subtracted.

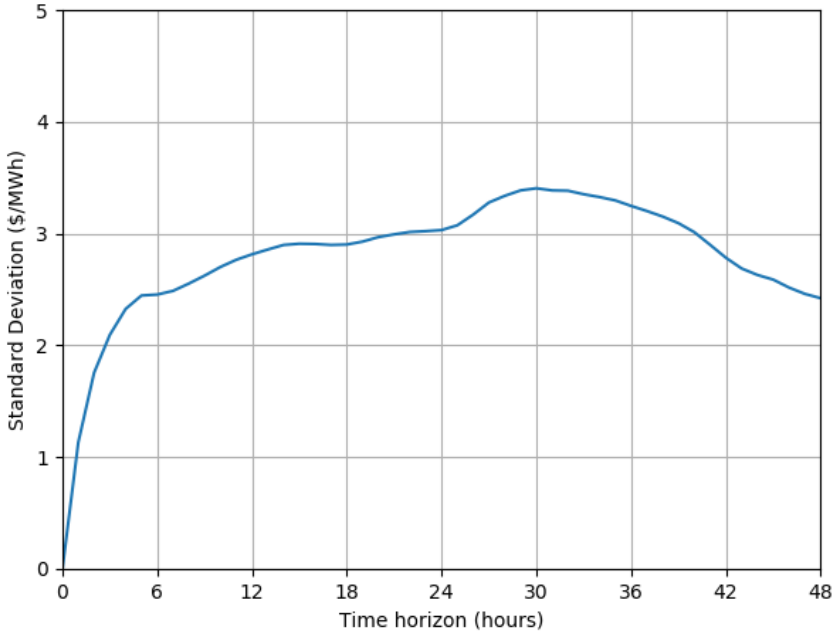

Figure 16: Standard deviation of spot-price forecasts as a function of time horizon. The number of data points used to calculate each standard deviation varies, with less data points available for longer time horizons.

conditions may warrant.

The magnitude of the peaks of the spot price data were altered subject to a spot price factor. First the average of the spot-price time series was taken and then subtracted from the time series. The residual is then mutliplied by the spot price factor, after which the average is added once again to the time series. This method was chosen to accord with the observation that the spot price errors were largely in the magnitude of the peaks. The spot price factors used are: [0.0625, 0.125, 0.25, 0.5, 1, 2, 4, 8, 16], and Figure 18 shows the resulting spot price time series used in the forecast. For the sake of inquiry, the spot price factors return much larger variations in spot price peaks than were observed in the errors from the ARIMA model displayed in Figure 18.

5.2 Variation of commitment schedule

Figure 19 gives the resultant commitment schedules, where the first 12 hours is unaffected due to the fact that it represents an assumed commitment that was theoretically set on the day before the optimisation was conducted. Each subplot represents the committed schedule over a range of spot price factors for a given DNI multiplier, that is represented in the associated title.

This study has the added bonus of representing the optimal schedule should the used DNI and spot price time series be a true representation of these factors. It allows us to view how the optimisation algorithm shifts generation subject to a wide range of spot price variation and total incident solar irradiation under clear sky conditions.

In the case of low to moderate DNI price multipliers, the energy generation schedule is altered with respect to the spot price factor in order to exploit spot price peaks. For

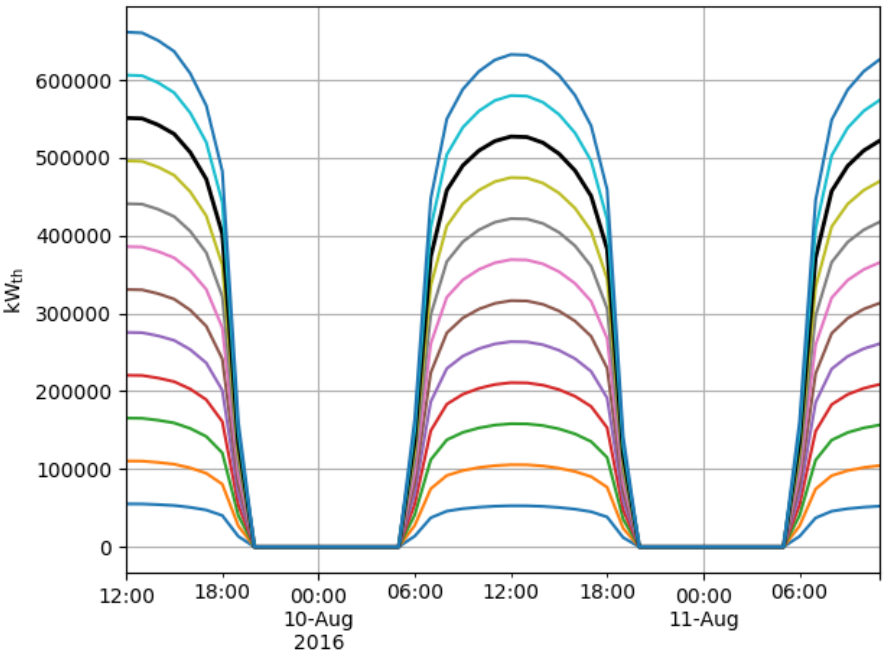

Figure 17: Figure to demonstrate the different thermal energy input values used as forecast time series for the scheduling optimisation. Here the original DNI forecast has been used as input to solar field model. Solar field efficiency affects the time series. The black time series represents the actual DNI measured over the simulation time interval.

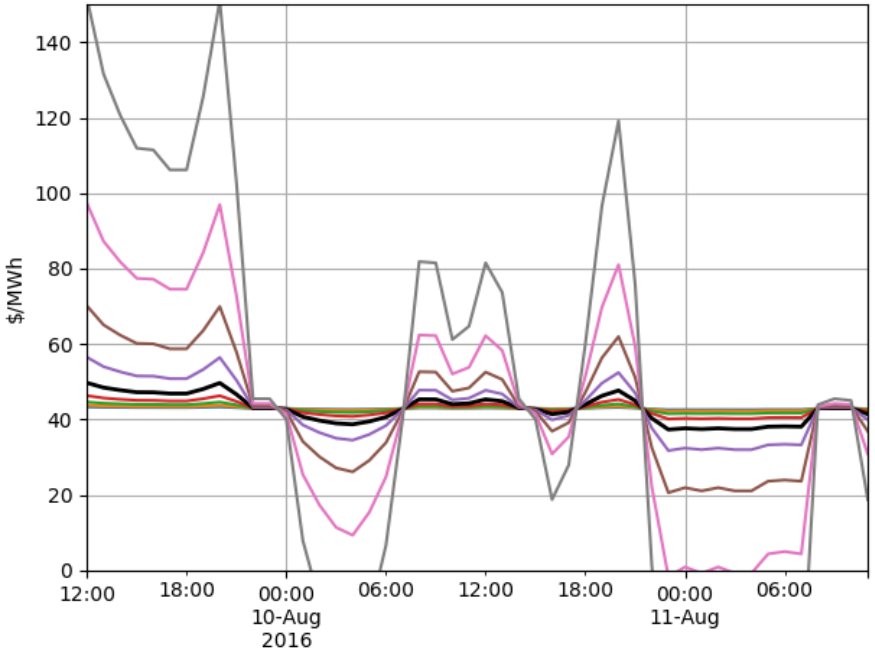

Figure 18: Figure to demonstrate the different SP values used as forecast time series for the optimisation. The black time series represents the actual spot price over the time interval of the simulation.

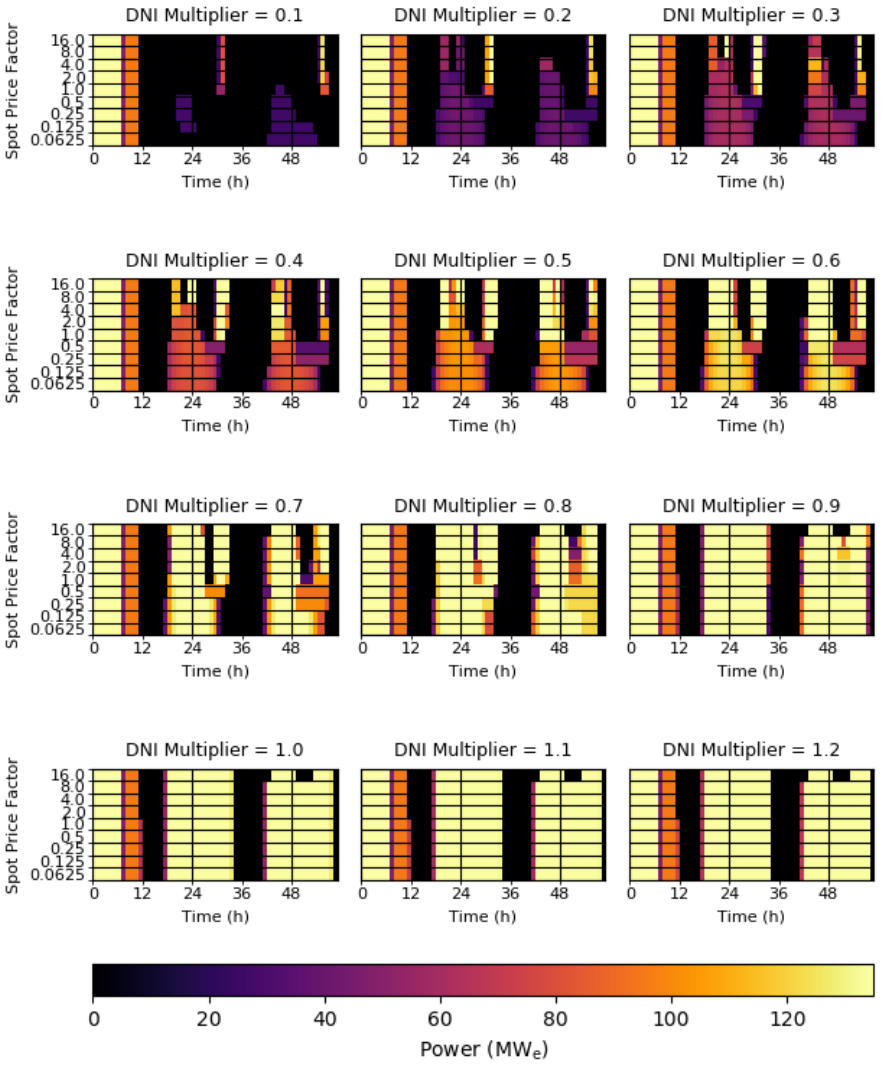

Figure 19: Generation schedule used for commitment subject to variations in the spot price and DNI that are imposed in order to represent a wide range of forecast errors. The time axis represents the time horizon, and not the hour of the day, and generation schedule begins at 12 noon on the 10th of August 2016.

relatively low spot price factors, which correspond to low spot price variability, the incentive to store for later generation is largely removed in favour of avoiding losses associated with storage and ramping the turbine up and down, the latter being defined by the cost factor $C_{\Delta P}$. For higher DNI multipliers, the total irradiance is higher and storage is used to distribute the generation over a wider time window in order to make full use of the large amount of incoming solar radiation that is subject to the bottleneck of maximum turbine output. The latter case is therefore less selective with respect to generation time, while still avoiding the price troughs associated with overnight generation.

5.3 Variation of actual generation schedule with changes in commitment

The range of different commitment schedules are used as inputs to the model for optimising the actual generation schedule using the measured solar energy input from Figure 8 and the actual spot price data of Figure 14. The simulations conducted use a real-time optimisation approach where the operational point for the subsequent hour of generation is determined using a forecast over the following 48 hours, assuming perfect knowledge of the forecast DNI and spot price, but subject to the erroneous generation commitments presented in Fig 19. Assuming perfect knowledge in this way isolates the effect of erroneous generation commitment, which is an important consideration in a market where generation commitments are made a day ahead.

What is most evident from these figures is that for the representative generation commitment penalty of $C_{\text{commit}} = 10$ Euros/MWh, the optimal generation schedule is largely unaffected by the range of different commitment time series that were used. In this case, with a relatively modest solar multiple of 1.5 and 4 storage hours, the amount of energy incident on the power plant is enough that the turbine must generate at full capacity for a majority of the available generation time.

For completeness, the revenues associated with these time series, along the commitment penalties, are presented in Appendix B. The sum of the revenues are presented in Figure 21. As expected from the negligible variations in the generations schedules presented in Figure 20, the gross revenue from the power plant for the different multipliers shows very little variation.

The penalties due to incorrect commitment as a function of the DNI multiplier and the spot price factor are shown in Figure 22. The DNI multiplier has the greatest effect on the subsequent penalty, as an increase in DNI with respect to that expected when commitment was made forces the plant to generate at a higher output in comparison to the commited schedule. The penalties represent, at most, approximately 15% of the revenue from the power plant for the chosen commitment penalty factor. This represents an upper limit of the penalty, as the extremes of the DNI multiplier and the spot price factor represent extremes in commitment schedule errors for this case study. It should be noted here than an increase in the commitment penalty factor C_{commit} should not imply a linear increase in the penalty, as the optimiser may determine a different schedule for larger penalties in order to avoid them.

Figure 23 shows the net income of the power plant as a function of the spot price factor and the DNI multiplier. This is the revenue of the power plant minus the penalties due to incorrect commitment, and the trend observed here roughly approximates the inverse trend of the penalties due to the fact that revenue is approximately constant across all spot price factors and DNI multipliers.

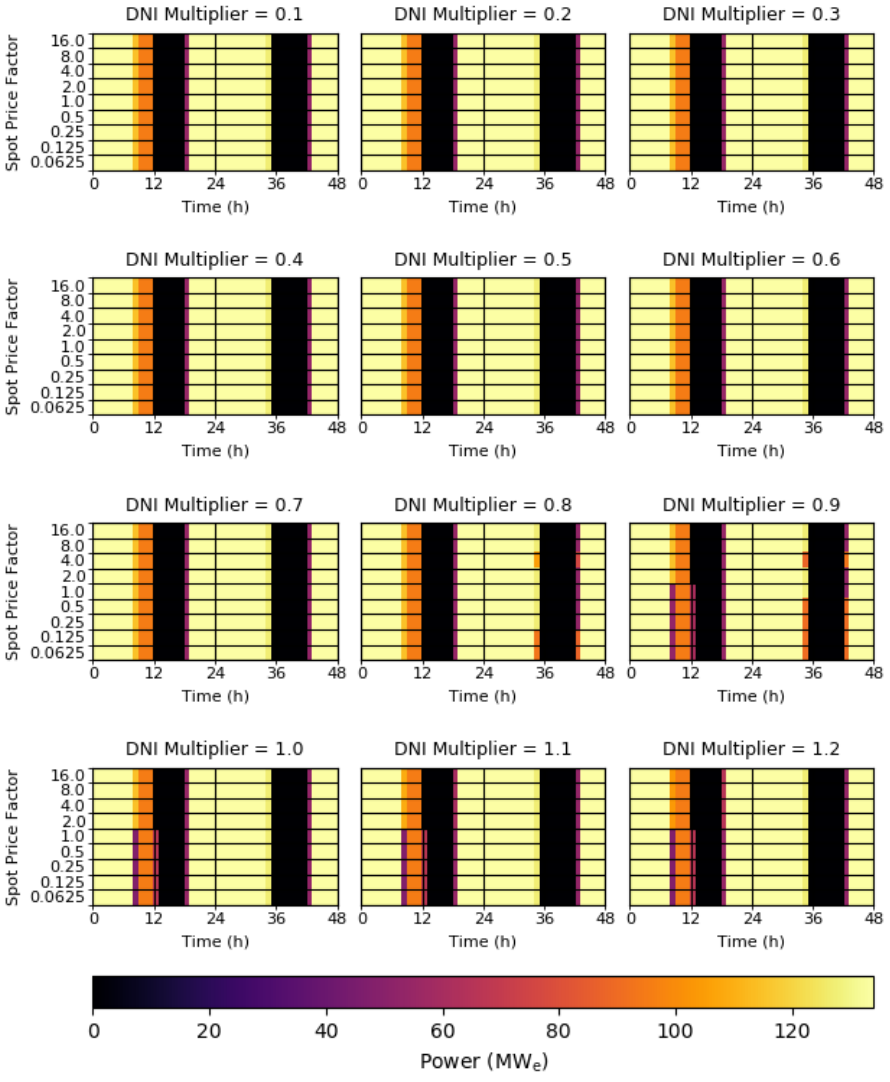

Figure 20: Optimal generation schedule subject to a range of erroneous generation commitments, subject to the actual DNI and spot prices, with operation made assuming perfect forecast knowledge. The spot price factor and the DNI multiplier labels represent those that were used to estimate the generation commitment.

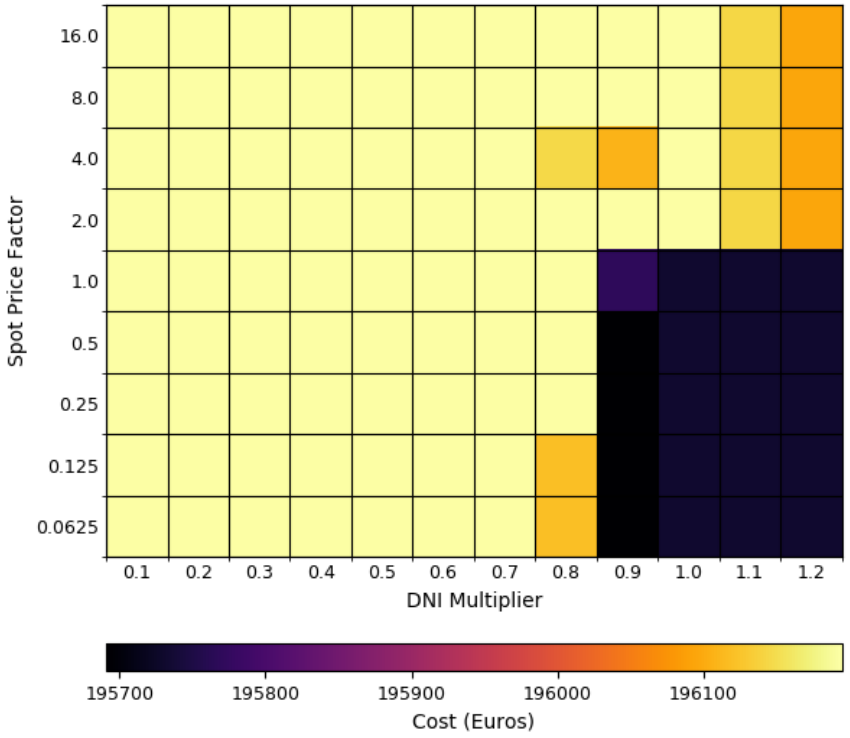

Figure 21: Sum of revenues ranging over spot price and DNI errors that were present when the commitment schedule was made.

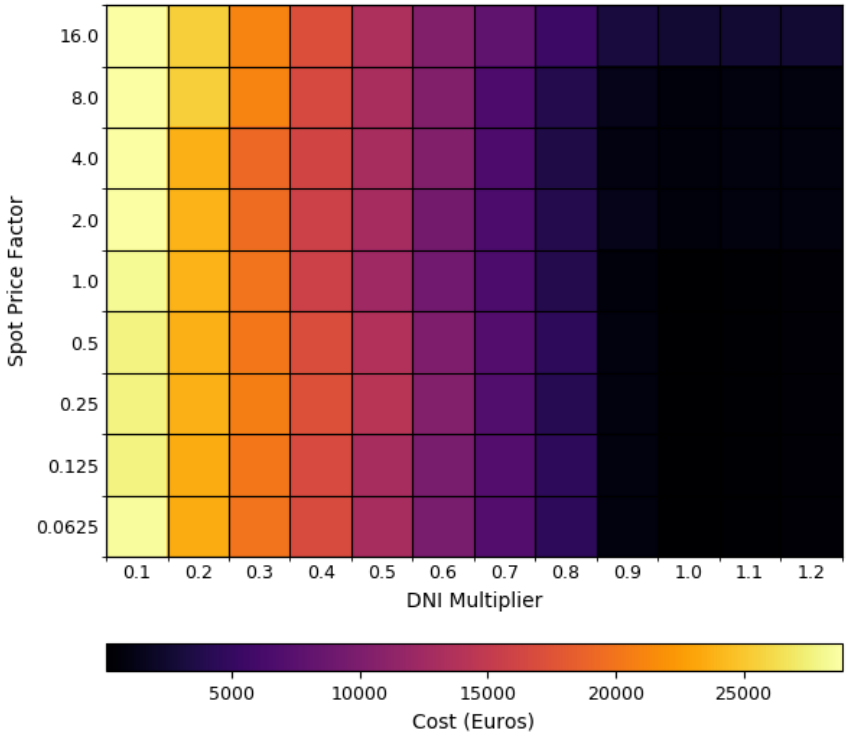

Figure 22: Sum of penalties ranging over spot price and DNI errors.

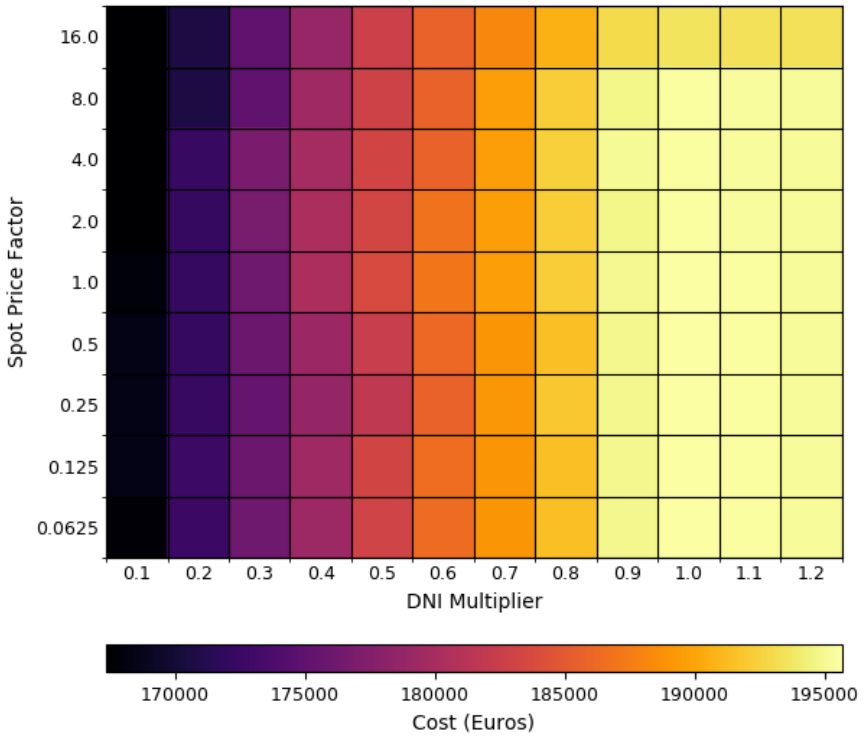

Figure 23: Sum of net revenue ranging over spot price and DNI errors.

Future work may focus on higher generation penalties, along with power plants that have lower solar multiples for which altering the generation schedule to match the commitment may be more advantageous.

6. Optimal operation using forecasts and CSP plant controller

In this section, we present real-time operation of the CSP power plant. At a given time step t, the generation schedule for the next two days is optimised according to the forecast DNI and spot price time series made at that time. Operation is then determined for $t+1$ subject to the expected operation over this time horizon. Due to the uncertainty in the forecasts, energy input to the power plant at $t+1$ may be different from the forecast value. A plant controller was therefore created that represents a real-time decision-making approach in order to account for deviations from the forecast power plant operation set point. This represents a formulation for operation of a CSP plant under uncertainty.

Energy from the receiver may either be directed to the storage tank or to the power block, with the possibility that some or all of the power to the power block comes from storage. A simplified summary of control approach follows[3]:

- Generation from storage should match the amount dictated by the optimiser.
- The ratio of the solar energy directed to generation over the solar energy directed to storage should be preserved.
  - When turbine output is maximised due high input solar energy, the ratio is not preserved. In this case, the turbine output is maximised and the

[3]A full logic diagram of the controller can be made available from the author on request

remainder is directed to storage.

- When the storage output is also maximised, the rest of the energy is discarded by defocusing the mirrors from the receiver.

- If the amount of input thermal energy is not enough to run the turbine, the power plant is shut down.

The operational set-point determined by the controller is fed into the initial conditions of the optimisation for the subsequent time step. This is performed recursively until the two days of operation have been simulated. The resultant generation time series is then compared to the ideal optimised generation time series that is calculated using the real measured data. The comparison allows to attribute a monetary value to the effects of both the uncertainties in the forecast data and the limitations of the plant controller on plant revenue.

Figure 24 shows the results from the optimised real-time operation using the rolling DNI and spot price forecasts with the CSP plant controller, in comparison to the ideal schedule optimised using the subsequent measured values.

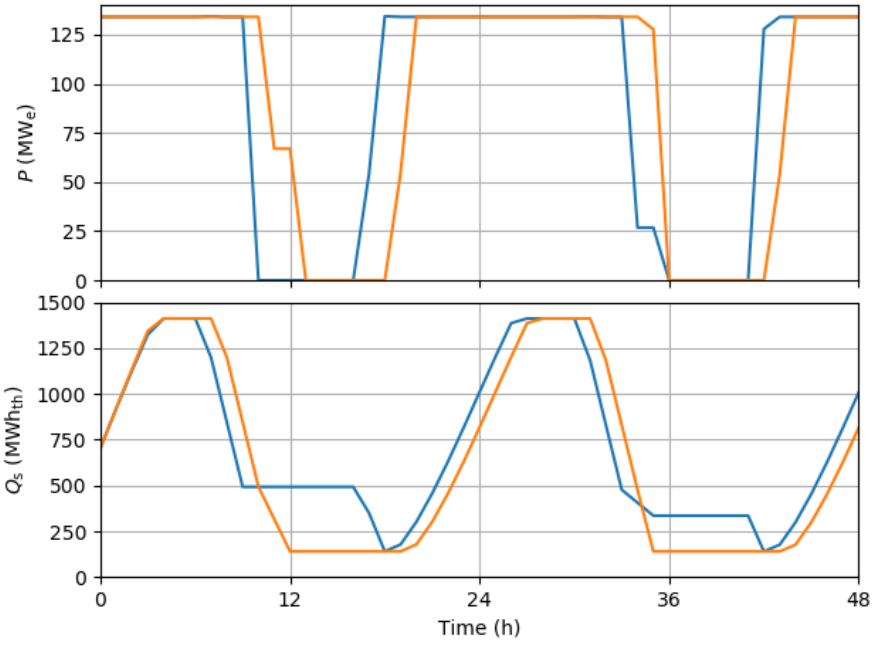

Figure 24: Results from the simulation using the forecast time series and the CSP plant controller to estimate best operation with uncertain information about future operation (blue) in comparison to the ideal optimised schedule calculated using the subsequent measured DNI and spot price values (orange).

The controller exhibits a tendency to cancel generation earlier in the day and to being earlier the following day. The reason for this is uncertain because it is confounded by both the presence of uncertainty in the real-time operation, and the fact that the perfect forecast has information up to 96 hours in advance that may influence the generation profile over the current time window.

The total revenue over the 48-hour operational window for the real-time optimisation case using the plant controller is \$1.941 $\times 10^5$ in comparison to the ideal case of \$1.965 $\times 10^5$, such that operating the CSP power plant using the forecast data achieved approximately

98.7% of the revenue in comparison to the ideal case.

Assuming that this is representative of the lost income due to uncertainty, an opportunity to increase plant revenue by 1.2% with respect to the real-time operation value exists, which may be significant once one accounts for the fraction of revenue that represents profit in a competitively priced power plant.

7. Conclusion

In this project, the Cyprus Institute has incorporated new methods for predicting aerosol concentrations in the local region in order to inform forecasts of direct normal irradiance suitable for use in concentrating solar power plant operational simulations. The forecast of DNI provided by the the Cyprus Institute represent an error of up to 0.5% up to a time horizon of 48 hours.

RWTH Aachen has first provided an estimate of the effect of systematically generated uncertainties in spot price and DNI data in order to investigate the influence of these uncertainties on penalties associated with deviations from a day-ahead commitment. The presented case study power plant had a solar multiple of 1.5 and 4 hours of storage, and clear-sky conditions were simulated in order to correspond to the measured time series provided by the Cyprus Institute over the time period of interest. Results indicate that uncertainties in the day ahead commitment are associated with an increase in penalties, but, that under an educated assumption of a deviation-from-commitment penalty of 10 Euros/MWh did not indicate a significant change in the generation schedule for the case study power plant.

RWTH Aachen then used a suite of rolling DNI forecasts, provided by the Cyprus institute, on an hourly basis with a time horizon of two days, along with forecasts of electricity spot price data generated in-house using an ARIMA model that predicts spot prices based on historical spot price data, as input to the CSP plant scheduling optimisation model. The ARIMA model is accurate is within 10% over a time horizon of two days. A plant controller heuristic was introduced in order to cope with deviations from the forecast input energy and associated optimal plant set point. The resulting simulated real-time operation of the power plant provided a schedule for plant operation that generated earlier in the day and shut down earlier in the evening. This may be the result of the limited forecast time horizon in comparison to the simulated ideal case. This may also be a result of limitation of the controller to deal with the uncertainties in the forecast data. Comparison of the real-time operation to the ideal case indicate that 98.7% of the maximal possible revenue has been achieved for this case study.

8. Future Work

This formulation for optimisation of plant operation under uncertainty can be further improved with the implementation of a robust controller in order to account for forecasted operation near the turbine operational limits and storage limits. This can be facilitated with the generation of ensemble forecasts from a NWP model in order to estimate the uncertainty envelope that should define the limits of DNI suitable for creating the robust model.

This can lead to further investigations of power plant operation in the case of variable DNI on cloudy days, which could cause more unpredictability for the plant controller and for the day ahead commitment.

References

M. Abdelkader, S. Metzger, B. Steil, K. Klingmueller, H. Tost, A. Pozzer, G. Stenchikov, L. Barrie, and J. Lelieveld. Sensitivity of transatlantic dust transport to chemical aging and related atmospheric processes. *Atmos. Chem. Phys*, 17:3799–3821, 2017.

M. Adbelkader, S. Metzger, R. E. Mamouri, M. Astitha, L. Barrie, Z. Levin, and J Lelieveld. Dust-air pollution dynamics over the eastern mediterranean. *Atmos. Chem. Phys*, 15:9173–9189, 2015.

R. Dominguez, L. Baringo, and A.J. Conejo. Optimal offering strategy for a concentrating solar power plant. *Applied Energy*, 98:316 – 325, 2012. ISSN 0306-2619. doi: http://dx.doi.org/10.1016/j.apenergy.2012.03.043. URL `http://www.sciencedirect.com/science/article/pii/S0306261912002619`.

Birk Kraas, Marion Schroedter-Homscheidt, and Reinhard Madlener. Economic merits of a state-of-the-art concentrating solar power forecasting system for participation in the spanish electricity market. *Solar Energy*, 93:244 – 255, 2013. ISSN 0038-092X. doi: https://doi.org/10.1016/j.solener.2013.04.012. URL `http://www.sciencedirect.com/science/article/pii/S0038092X13001527`.

S. Metzger, B. Steil, L. Xu, J.E. Penner, and J. Lelieveld. New representation of water activity based on a single solute specific constant to parameterize the hygroscopic growth of aerosols in atmospheric models. *Atmos. Chem. Phys*, 12:5429–5446, 2012.

S. Metzger, M. Abdelkader, K. Klingmueller, B. Steil, and J. Lelieveld. Comparison of metop pmap version 2 aod products using model data, final report eumetsat itt 15/210839. Technical report, Max Planck Institute for Chemistry, Department of Atmospheric Chemistry, 2016a.

S. Metzger, B. Steil, M. Abdelkader, Klingmueller, L. Xu, J.E. Penner, C. Fountoukis, A. Nenes, and J. Lelieveld. Aerosol water parameterization: A single parameter framework. *Atmos. Chem. Phys*, 16:7213–7237, 2016b.

Corey J. Noone, Manuel Torrilhon, and Alexander Mitsos. Heliostat field optimization: A new computationally efficient model and biomimetic layout. *Solar Energy*, 86(2):792 – 803, 2012. ISSN 0038-092X. doi: 10.1016/j.solener.2011.12.007. URL `http://www.sciencedirect.com/science/article/pii/S0038092X11004373`.

A. Section 1

```
int: N_T;        %number of timesteps
int: N_commit;
float: C_commit;
float: T_len;      %length of each timestep (h)
float: T_up;   %minimum down-time for the solar power plant (h)
float: T_down;   %minimum up-time of the solar power plant (h)
int: L;
int: M;

int: N_on;
int: N_off;
int: U_0;       %initial commitment status of the generation unit: 1 if online, 0 otherwise

float: eta_tank;  %storage efficiency
float: eta_cycle;  %power cycle efficiency

float: P_max;  %capacity of the concentrating solar power plant (MWe)
float: P_min;  %minimum electrical output from the power block
float: Q_smax; %Energy capacity of the thermal energy storage (MWhth)
float: Q_smin; %minimum energy storage
float: R_dis;  %ramp-down limit for discharging the thermal energy storage (MWe/h)
float: R_chg;  %ramp-up limit for discharging the thermal energy storage (MWe/h)

%initial conditions
float: Q_s0;    %initial thermal energy in tank
float: P_0;      %initial electric power output of the CSP plant
float: Qdot_re0;   %initial thermal power from the field to the cycle
float: Qdot_se0;   %initial thermal power from the storage to the cycle
float: Qdot_rs0;   %initial thermal power from the solar field to storage
float: Qdot_pass0; %initial thermal power being bypassed from storage or generation
float: C_deltaP;  %cost in euros per MWh for changing the output of the turbine.

array[1..N_T] of float: SP;
array[1..N_T] of float: Q_SF;
array[1..N_commit] of float: P_commit;
array[1..N_T+1] of var float: P;        %electric power output of the CSP plant
array[1..N_T+1] of var float: Qdot_re;     %electric power directly produced from the solar field
array[1..N_T+1] of var float: Qdot_rs;     %thermal power from the solar field to storage
array[1..N_T+1] of var float: Qdot_se;     %thermal power from storage used for generation
array[1..N_T+1] of var float: Qdot_pass;   %thermal power bypassed from storage or generation
array[1..N_T+1] of var float: Q_s;      %thermal energy in tank at end of interval
array[1..N_T] of var float: deltaP_abs; %absolute value of the change in electricity
array[1..N_commit] of var float: delta_commit_abs;
array[1..N_T+1] of var int: U;         %binary variable. Plant on = 1, plant off = 0

constraint P[1] = P_0;
constraint Qdot_re[1] = Qdot_re0;
constraint Qdot_se[1] = Qdot_se0;
constraint Qdot_rs[1] = Qdot_rs0;
constraint Qdot_pass[1] = Qdot_pass0;
constraint Q_s[1] = Q_s0;
constraint Q_s[N_T+1] = Q_s0;
constraint U[1] = U_0;
```

```
constraint forall(t in 2..N_T+1)(P[t] >= P_min * U[t]);
constraint forall(t in 2..N_T+1)(P[t] <= P_max * U[t]);
constraint forall(t in 2..N_T+1)(Q_s[t] >= Q_smin);
constraint forall(t in 2..N_T+1)(Q_s[t] <= Q_smax);
constraint forall(t in 2..N_T+1)(Qdot_rs[t] >= 0);
constraint forall(t in 2..N_T+1)(Qdot_re[t] >= 0);
constraint forall(t in 2..N_T+1)(Qdot_se[t] >= 0);
constraint forall(t in 2..N_T+1)(Qdot_pass[t] >= 0);
constraint forall(t in 2..N_T+1)(U[t] <= 1);
constraint forall(t in 2..N_T+1)(U[t] >= 0);

constraint forall(t in 2..N_T+1)(Q_SF[t-1] = Qdot_re[t] + Qdot_rs[t] + Qdot_pass[t]);
constraint forall(t in 2..N_T+1)(P[t] = eta_cycle * (Qdot_re[t] + Qdot_se[t]));
constraint forall(t in 1..N_T)(Q_s[t+1] = Q_s[t] + T_len * (Qdot_rs[t+1] - Qdot_se[t+1] / eta_tank));
constraint forall(t in 1..N_T)(eta_tank * eta_cycle * (Qdot_se[t+1] - Qdot_se[t]) <= R_dis);
constraint forall(t in 1..N_T)(eta_cycle * (Qdot_rs[t+1] - Qdot_rs[t]) <= R_chg);

constraint forall(t in 2..N_T+1)((P[t] - P[t-1]) <= deltaP_abs[t-1]);     %from Vasallo and Bravo
constraint forall(t in 2..N_T+1)((P[t-1] - P[t]) <= deltaP_abs[t-1]);     %from Vasallo and Bravo

constraint forall(t in 2..N_commit+1)((P_commit[t-1] - P[t]) <= delta_commit_abs[t-1]);
constraint forall(t in 2..N_commit+1)((P[t] - P_commit[t-1]) <= delta_commit_abs[t-1]);

constraint sum(t in 2..L+1)(1 - U[t]) = 0;
constraint forall(t in L+2..N_T-round(T_up/T_len)+2)
    (sum(j in t..t+round(T_up/T_len)-1)(U[j]) >= T_up/T_len * (U[t] - U[t-1]));
constraint forall(t in N_T-round(T_up/T_len)+3..N_T+1)
    (sum(j in t..N_T+1)(U[j] - (U[t] - U[t-1])) >= 0);

constraint sum(t in 2..M+1)(U[t]) = 0;

constraint forall(t in M+2..N_T-round(T_down/T_len)+2)
    (sum(j in t..t+round(T_down/T_len)-1)(1 - U[j]) >= T_down/T_len * (U[t-1] - U[t]));

constraint forall(t in N_T-round(T_down/T_len)+3..N_T+1)
    (sum(j in t..N_T+1)(1 - U[j] - (U[t-1] - U[t])) >= 0);

solve maximize sum(t in 2..N_T+1)
    (T_len * (P[t] / 1e3 * SP[t-1]) - T_len * C_deltaP * deltaP_abs[t-1] / 1e3) -
    sum(t in 1..N_commit)(T_len * C_commit * delta_commit_abs[t] / 1e3) -
    sum(t in 2..N_T+1)((N_T + 1 - t) * Qdot_pass[t]) / 10000000 -
    sum(t in 2..N_T+1)(Qdot_rs[t]) / 100000;
```

B. Revenues and penalties associated with the erroneous commmitments

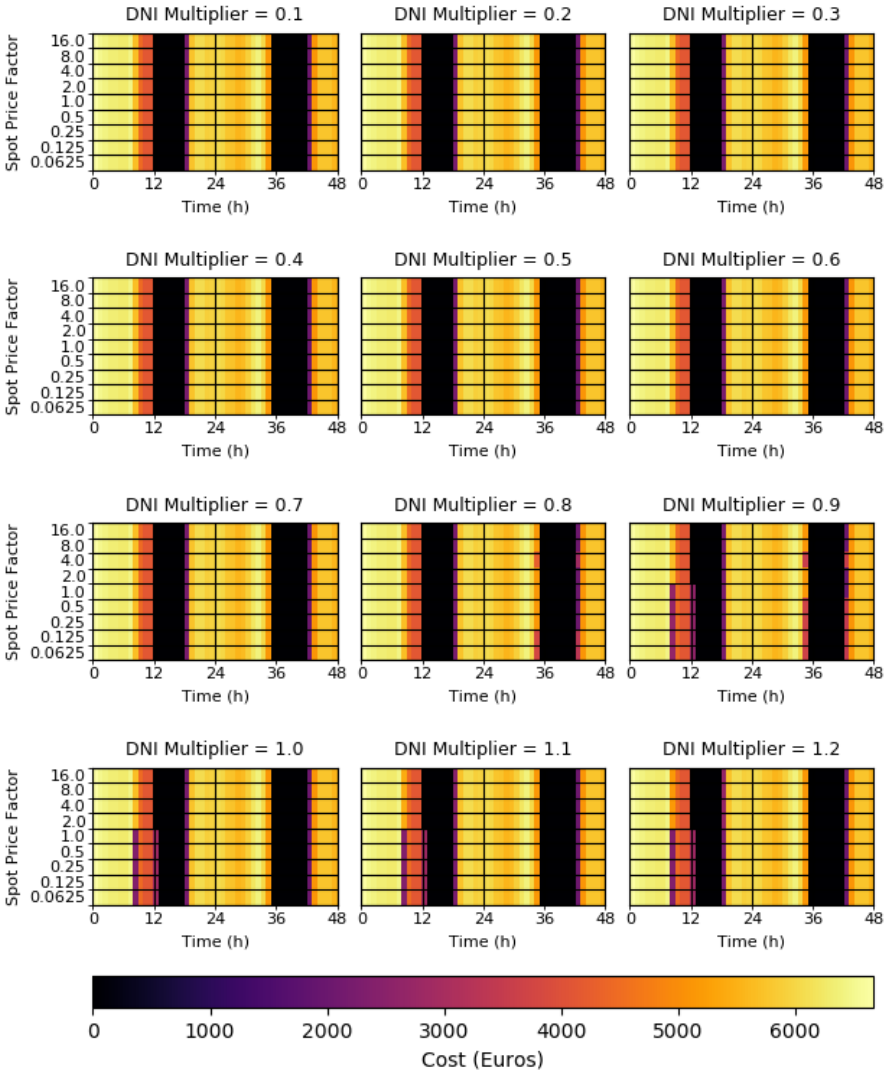

Figure 25: Revenue time series.

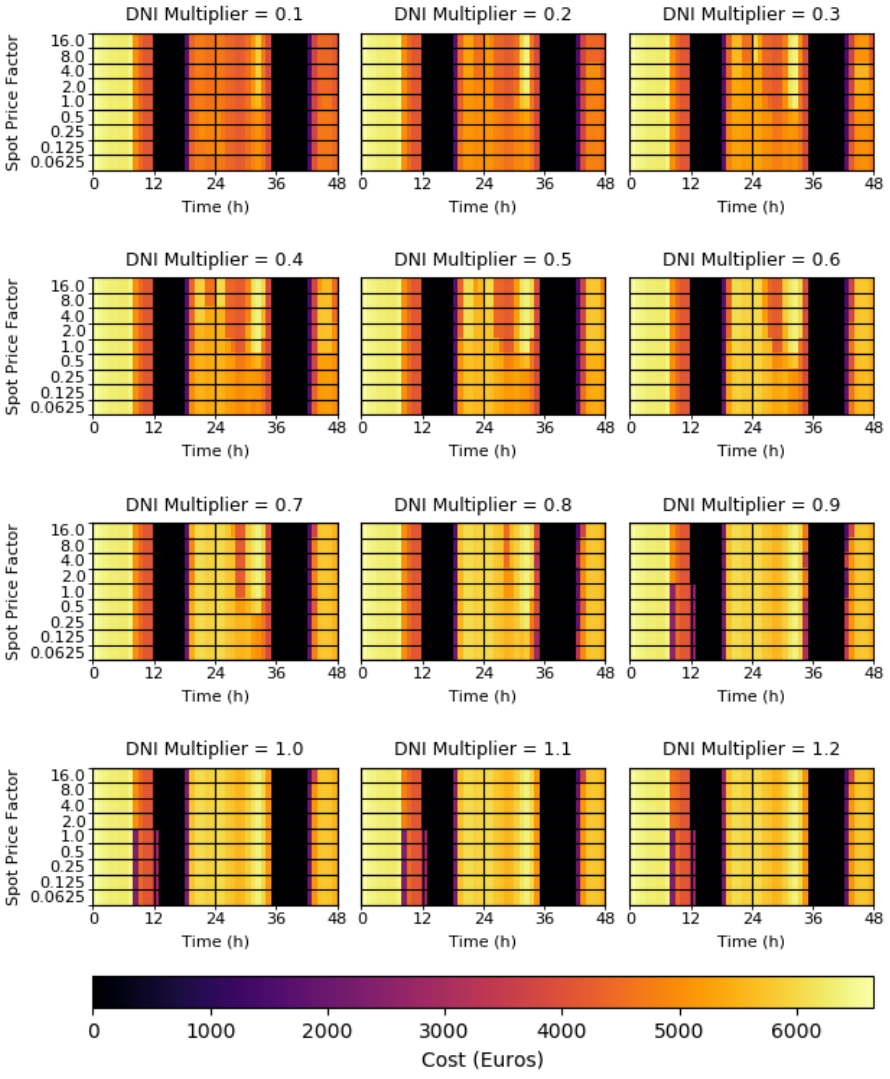

Figure 26: Net revenue.

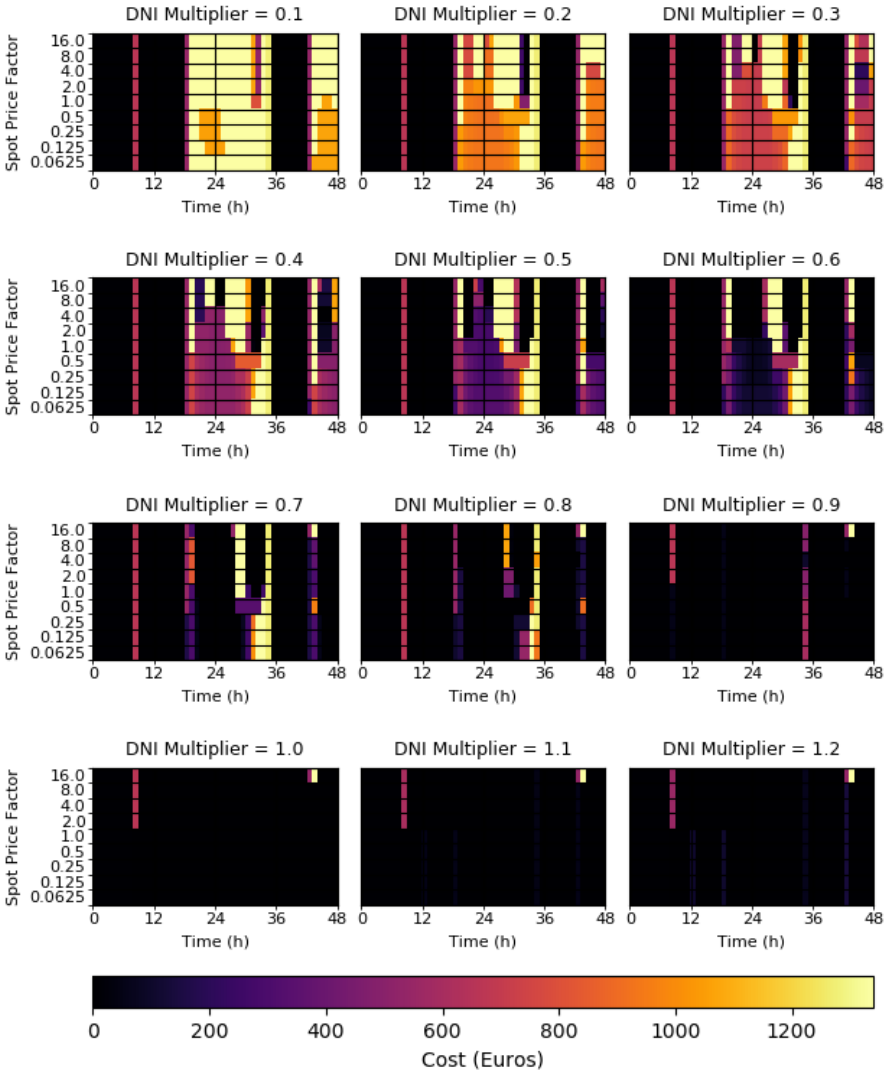

Figure 27: Penalties.